Versatile quantum-enabled telecom receiver

M. V. Jabir,[1] N. Fajar R. Annafianto,[1] I. A. Burenkov,[1,2] M. Dagenais,[3] A. Battou,[1] and S. V. Polyakov[1,4]

AFFILIATIONS

[1]National Institute of Standards and Technology, Gaithersburg, Maryland 20899, USA
[2]Joint Quantum Institute, University of Maryland, College Park, Maryland 20742, USA
[3]Department of Electrical and Computer Engineering, University of Maryland, College Park, Maryland 20742, USA
[4]Department of Physics, University of Maryland, College Park, Maryland 20742, USA

ABSTRACT

We experimentally demonstrate a quantum-measurement-based receiver for a range of modulation schemes and alphabet lengths in a telecom C-band. We attain symbol error rates below the shot noise limit for all the studied modulation schemes and the alphabet lengths $4 \leq M \leq 16$. In doing so, we achieve the record energy sensitivity for telecom receivers. We investigate the trade-off between energy and bandwidth use and its dependence on the alphabet length. We identify the combined (energy and bandwidth) resource efficiency as a figure of merit and experimentally confirm that the quantum-inspired hybrid frequency/phase encoding has the highest combined resource efficiency.

I. INTRODUCTION

Communication with light plays a pivotal role in enabling the global Internet because optical technology offers faster, more energy-efficient data exchange compared to all-electronic networks. In optical communications, digital information is encoded into a certain set of states of light that comprise a communication alphabet. The optical receiver is the key component of a communications link. The receiver decodes information from the input optical signal. Depending on the length of the alphabet, each optical symbol can yield one or more bits. The energy sensitivity of a receiver defines the minimal optical power at the input of the receiver required for reliable communication. Such sensitivity is characterized by the symbol error rate (SER) or the probability to receive a symbol incorrectly for a given input energy per communicated optical symbol. Quantum properties of light set the fundamental limit on the minimum error rate known as shot noise limit (SNL) for given input energy and the alphabet is accessible to any classical measurement. In other words, this fundamental limit defines the minimum bound on energy and bandwidth required for reliable communication using classical receivers. On the other hand, the quantum theory sets a much lower error bound known as the Helstrom bound (HB).[1] The HB defines the smallest error allowed by the laws of quantum mechanics and may be accessible to quantum measurement. Receivers equipped with quantum measurement and achieving the SER below the SNL are called "quantum receivers" hereafter. The first theoretical proposal of the quantum receiver that can reach the HB was the one by Dolinar.[2] The Dolinar receiver reaches the HB for a binary alphabet only, i.e., when a symbol encodes one bit. Other receiver arrangements[3] can also reach HB for binary alphabets. While reaching the HB for longer alphabets is theoretically possible,[4] an experimental implementation remains challenging. On the other hand, multiple methods that can be readily implemented and performed below the absolute SNL were proposed.[5–11] A number of experiments demonstrated the SER below the SNL.[12–27]

Until very recently, most experimental demonstrations considered binary and $M = 4$ alphabets. A modulation scheme also plays an important role in defining communication resources. Because coherent states of light are used to encode the information bit,[28] frequency, phase, and/or amplitude are accessible parameters. To optimize the resource use given the practical limitations of the communication channel, both the encoding scheme and the alphabet length are important. Until very recently, the quantum receivers were applied to phase-shift keying (PSK) alphabets where symbols differ by phase[12–21,26,27] and pulse-position modulation (PPM) where symbols differ by a time shift.[8,35] Finally, nearly all the experimental demonstrations of quantum receivers have been done at visible wavelengths[29] with the exception of Refs. 26 and 27. Yet, the practical use of a quantum receiver requires implementation at telecom wavelengths.

Here, we report on the first photon arrival time-resolving quantum receiver that operates in the telecom C band. This receiver resolves and uses photon arrival times to improve energy sensitivity

for a range of encodings and a range of alphabet lengths, which makes this receiver versatile. In particular, we test our receiver with $M = 4$, 8, and 16 alphabets. Also, we employ the legacy PSK, the novel coherent frequency shift keying (CFSK),[11,23,24] and hybrid frequency phase shifted keying (HFPSK)[30] that exploit the quantum properties of coherent states and single-photon detection to achieve advantageous resource use. Here, we measure that the CFSK yields the lowest energy per bit while HFPSK offers the favorable combined energy and bandwidth figure of merit. We present the first experimental evidence of below the SNL error rates achieved in the telecom band for long $M =$ 8, 16 communication alphabets and also demonstrate the lowest SER for $M = 4$ with the input energy of just 1 photon/bit.

To do so, we built the time-resolving receiver, cf. Ref. 23, using an efficient superconducting nanowire single photon detector (SNSPD) with high efficiency at telecom wavelengths and a field programmable gate array (FPGA). This receiver is versatile by design; only FPGA firmware is changed to switch the alphabet length or encoding method.

This work enables the practical use of quantum receiver technology for telecommunications, particularly targeting energy-efficient and bandwidth-efficient communications with longer alphabets, i.e., when more than two bits are communicated per each optical state transmission. By optimizing bandwidth and energy use, potentially, a quantum-measurement-enabled receiver at telecom can overcome the capacity crunch due to exponential demand for the resources.[31]

II. MODULATION SCHEMES AND ENCODINGS

In this work, we consider alphabets of coherent states with frequency and phase modulations. Most generally, consider an M-ary alphabet of rectangular coherent optical pulses $\{|\alpha(\omega_i, \theta_{ij})\rangle\}$ with duration T. For each frequency $\omega_i = \omega_0 + (i-1)\Delta\omega, i \in 1, \ldots, M_f$, there can be the initial phase $\theta_{ij} = (i-1)\Delta\theta_f + (j-1)\Delta\theta_{ph}$ where $j \in 1, \ldots, M_{ph}$ and $\Delta\theta_{ph} = 2\pi/M_{ph}$ such that $M = M_f \times M_{ph}$. Therefore, for each M-ary alphabet, there can be several encodings depending on values of M_f and M_{ph}. This family of modulation schemes contains a legacy PSK when $M_f = 1$ and $M_{ph} = M$, and a CFSK when $M_f = M$ and $M_{ph} = 1$. Other encodings require both frequency and phase modulations and are called hybrid encodings (HFPSK). Since we aim to reduce the bandwidth usage, here we are particularly interested in small frequency detunings such that the adjacent frequencies are non-orthogonal: $\Delta\omega T < 2\pi$.

Figure 1(a) shows constellation diagrams of three possible encoding schemes for the alphabet length of $M = 4$ corresponding to $\log_2(4) = 2$ bits per symbol. Filled circles represent symbols, whose color represents the frequency and the angular position of a circle represents the phase shift at the beginning of the pulse. The first constellation corresponds to the CFSK modulation scheme, where all symbols have a different frequency $M = M_f = 4$, $M_{ph} = 1$. The second constellation corresponds to $M_f \times M_{ph}$—HFPSK modulation scheme in which symbols are encoded in two frequencies and two phases, $M_f \times M_{ph} = 2 \times 2$. The last one is the traditional PSK, where all symbols are encoded as phases of a single carrier frequency $M_f = 1$, $M = M_{ph} = 4$. Figures 1(b) and 1(c) show possible encodings for $M = 8$ corresponding to $\log_2(8) = 3$ bits per symbol and $M = 16$ corresponding to $\log_2(8) = 4$ bits per symbol. For $M = 8$, there are four encoding schemes of which two are HFPSKs. Similarly, for $M = 16$, there are five encoding schemes of which three are HFPSKs. The theory of

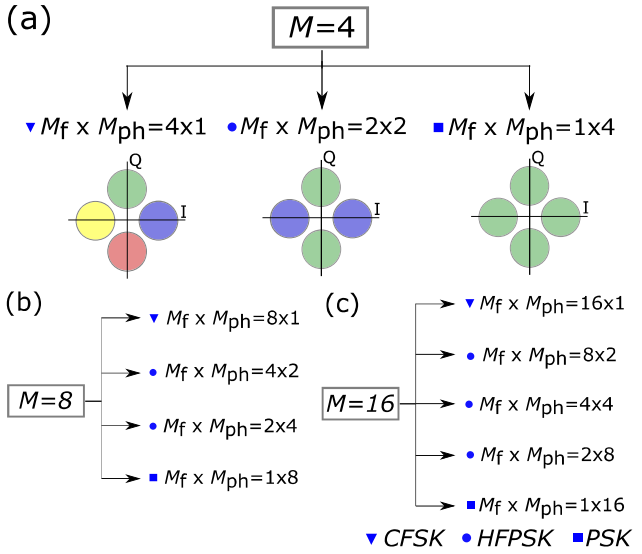

FIG. 1. Multiple encoding schemes for alphabet lengths of (a) $M = 4$, (b) $M = 8$, and (c) $M = 16$. Constellation diagrams are shown for $M = 4$ encodings. Filled circles represent symbols, color represents the frequency, and the angular position of a circle represents the phase shift at the beginning of the pulse. Solid triangle, circle, and square markers represent the CFSK, HFSPK, and PSK modulation schemes, respectively, and are used in other figures to identify the modulation scheme.

HFPSK alphabets including their SNLs and HBs and their comparison to CFSK and PSK is considered elsewhere.[30]

III. THE VERSATILE TELECOM QUANTUM RECEIVER

The experimental testbed for the quantum telecom-receiver platform is shown in Fig. 2(a). A fiber-coupled C-band laser (at $\approx$1.55 μm) is sent to a 90:10 fiber beam splitter (FBS-1). The output with higher intensity is sent to the reference beam preparation module where the beam is controlled by an acousto-optic modulator (AOM) and back-propagated through the testbed to interferometrically stabilize the transmitter–receiver arrangement. The other part of the beam from the FBS-1 is sent to the stabilized transmitter–receiver arrangement. The 99:1 FBS-2 sends 1% of the beam intensity into the transmitter that prepares the input signal and 99% into the telecom receiver to prepare the local oscillator (LO). The telecom receiver is comprised of the LO preparation module, the beam-splitter FBS-3, the fiber polarization controller (FPC), the SNSPD, and the FPGA [bounded by a gray border in Fig. 2(a)]. The transmitter and the LO preparation modules are identical, comprised of an AOM in a double-pass configuration,[32] two half-wave plates (HWP), a polarizing beam splitter (PBS), a quarter-wave plate (QWP), and a mirror [shown in the inset, Fig. 2(a)]. Depending on a modulation protocol, both phase and frequency can be modulated. The output from the transmitter and the LO is combined at the FBS-3 with a 99:1 intensity ratio and sent to the SNSPD. The electrical pulse generated after each photon detection at the SNSPD is sent to the FPGA for time-stamping, computing Bayesian probabilities, and hypotheses selection, cf. Ref. 23. The digital-to-analog converter (DAC) attached to the FPGA is used to generate sine RF signals for driving both AOMs. Also, the FPGA

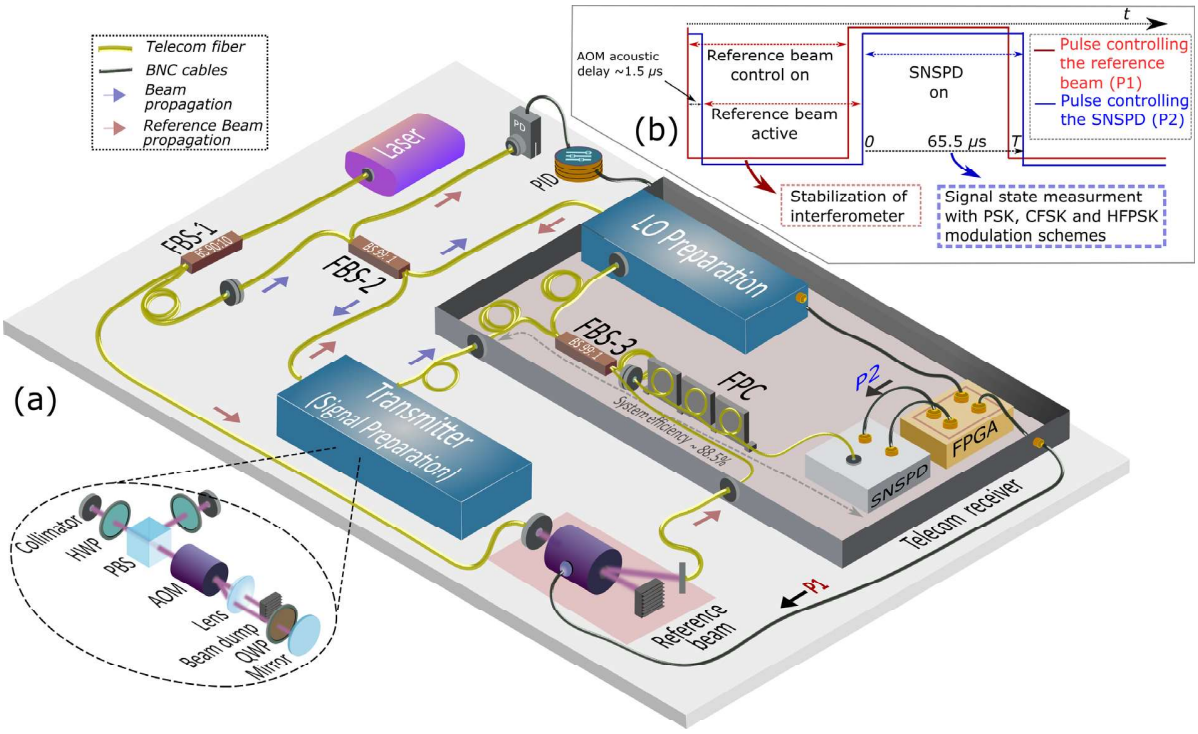

Fig. 2. The experimental testbed for the versatile quantum receiver. (a) The optical layout of the state discrimination testbed remains unchanged for all modulation schemes and alphabet lengths considered in this manuscript. (b) Controlling pulse for the reference beam (red) and the temporal gating of the SNSPD (blue).

determines the received state and compares it with the input state to determine if the state discrimination was successful. To determine the system efficiency, the input to the telecom receiver is defined as the input of the FBS-3 and marked with the gray dashed arrow, Fig. 2(a).

The reference beam is turned on and off using the AOM with a square pulse P1 (50% duty cycle) generated by FPGA, shown in red in Fig. 2(b). During the negative pulse cycle, the strong reference beam is sent to the transmitter–receiver interferometer arrangement and generates the error signal on a conventional photodiode (PD). PD output is used as an error signal for a proportional integral differential (PID) controller driving a piezo element attached to a mirror in the LO preparation setup and allows phase stabilization of the interferometer. Due to the acoustic delay in the AOM, the reference beam enters and leaves the interferometer with a 1.5 μs lag. To avoid the back-reflected light from the reference beam blinding the SNSPD, we use another square pulse P2 (50% duty cycle) with the offset of 1.5 μs [shown in blue in Fig. 2(b)] to gate the SNSPD. We turn the SNSPD off when the reference beam is active. This gating enables the use of the same laser to stabilize the interferometer and prepare the signal and the LO light, thus significantly simplifying the setup. For instance, the laser does not need to be locked to the external frequency standard. The raw estimated visibility of the transmitter–receiver interferometer reaches 99.4% (see Appendix A for more details). The measured detection efficiency of the SNSPD is 95.7(5)%. The total system efficiency of the telecom receiver is 88.5(5)% and it takes into account optical loss due to FBS-3, PC, fiber, and fiber connectors (see Appendix B for more details).

To identify the input signal state, both the signal and LO that correspond to the arbitrarily chosen initial hypothesis are sent to the FBS-3. The hypothesis is intended to produce the LO that displaces the input signal to the vacuum if the states of the hypothesis and the signal are the same. However, any incorrect hypothesis produces a non-vacuum state at the output and can result in photon detection. Every time a photon is detected, an electrical pulse is sent to the FPGA. The hypothesis is updated using the time of photon arrival and Bayesian inference.[11,23,24] It is to be noted that this receiver updates the hypothesis and displaces the signal with the minimal possible latency after each photon detection. At the time T, the current most likely hypothesis represents our best knowledge about the input signal state. If the current hypothesis matches the signal, discrimination is considered successful; otherwise, an error is registered. Modulation schemes and alphabet lengths are changed by reprograming the FPGA and no change in the physical layout is needed. All the experimental results are obtained for the detuning parameter $\Delta\omega T = \pi$, where $\Delta\omega \sim 2\pi \cdot 7629$ Hz and T = 65.5 μs.

IV. RESULTS AND DISCUSSION

A. Performance beyond the SNL

To demonstrate the quantum advantage of our telecom receiver, we have measured the symbol error rate (SER) for different modulation schemes: CFSK, PSK, and HFPSK, and compared it to the classical (SNL) and quantum (HB) limits. We point out that those fundamental limits are defined in terms of SER. Bit error rate (BER)

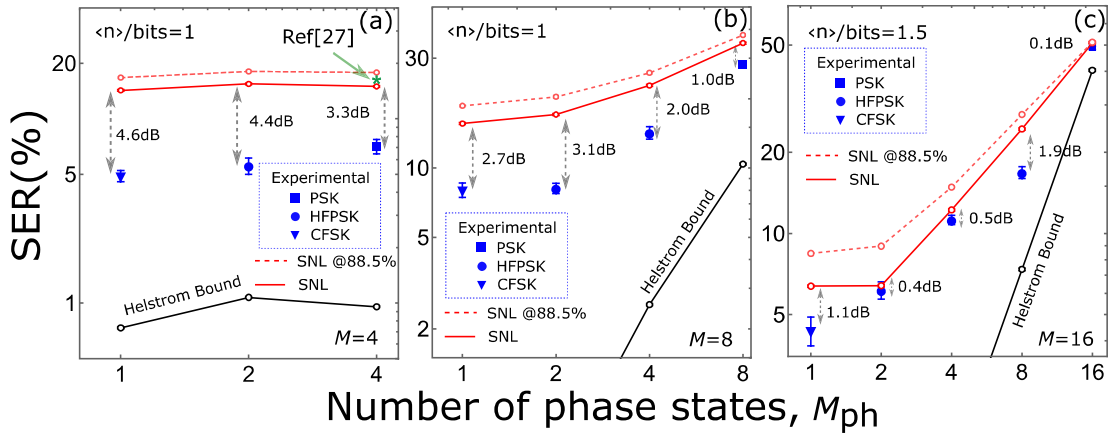

Fig. 3. Experimentally measured SER vs number of phase states, M_{ph} for different alphabet modulations and lengths (a) $M=4$, (b) $M=8$, and (c) $M=16$. Solid triangle, circle, and square markers represent the CFSK, HFPSK, and PSK modulation schemes, respectively. Red open dots connected with solid lines and dashed lines represent the absolute SNL and the adjusted SNL for our system efficiency, respectively. Black line—Helstrom Bound. All connecting lines are guides for the eye.

may be helpful for practical purposes. However, for non-binary alphabets, calculating BER requires a set of extra assumptions, such as a particular encoding of information into physical states and a particular distribution of errors. Making such assumptions limits generality and is beyond the scope of this work. To show the energy sensitivity of our receiver, here we choose input signal energy of ≈1 photon per bit for the alphabet lengths $M=4$ and 8 and ≈1.5 photons per bit for $M=16$. In Fig. 3, we plot SER versus number of phase states ($M_{ph}=M/M_f$) from 1 to 16. Figures 3(a)–3(c) show the quantum advantage of different modulation schemes for $M=4$, 8, and 16, respectively. To compare our receiver's performance to that of classical receivers, we also plot the corresponding SNLs: one SNL limit is adjusted for our system efficiency and the other one assumes the ideal classical detection with no loss—the absolute SNL. The SNLs are optimized for the phase parameter so that we can compare our experimental results with the best possible classical receiver with the matched encoding and the same input signal energy (cf. Ref. 11).

The quantum advantage is given by the ratio of the experimentally measured SER versus shot noise limited SER at given input energy and shown in decibels (dB) in Fig. 3. The best experimentally attained quantum advantage of all the encodings is given in Table I along with the input energy where the best advantage has been achieved. Note that all the encodings attain the SER below the absolute SNL. The CFSK has a higher quantum advantage among other modulations, which is not surprising because CFSK was designed to take the maximal advantage of a time-resolving displacement-based quantum receiver. Also, the highest advantage is obtained for $M=4$ protocols, while the lowest advantage is for $M=16$ protocols. This is because of the saturation of the performance of our receiver with input energy caused by a rather long latency time between registering a photon and switching the LO (which in our case is ∼1.5 μs). The latency is purely due to the technical implementation, e.g., the delay in the AOM due to the speed of sound. This latency can be therefore significantly improved by using electrical modulators.[33]

In comparing with the previous experimental results for PSK with $M=4$ at the telecom, we report the SER improvement of at least twofold compared to the previous record [green asterisks in Fig. 4(a)].[27]

Table I. Experimentally attained performance of our receiver with different encodings and alphabet lengths. The best quantum advantage over the ideal classical receiver is given by the smallest ratio of experimentally measured SER_E to the theoretical shot noise limited SER (SER_{SNL}) shown in decibels (dB). The statistical uncertainty in SER is one standard deviation. The $\langle n\rangle/\log_2 M$ is the average number of photons per bit (photons/bit) of the input signal where this minimum occurs.

	M_f	M_{ph}	SER_E/SER_{SNL} (dB)	$\langle n\rangle/\log_2 M$
$M=4$	4	1	−9.1(9)	2.8
	2	2	−5.1(4)	1.6
	1	4	−4.9(4)	1.7
$M=8$	8	1	−5.8(4)	2.2
	4	2	−3.2(3)	1.3
	2	4	−2.2(2)	1.5
	1	8	−2.9(3)	2.5
$M=16$	16	1	−1.3(3)	1.4
	8	2	−1.2(2)	1.1
	4	4	−0.5(1)	0.8
	2	8	−2.0(2)	2.7
	1	16	−1.8(2)	4.9

Note here that the receiver of Ref. 27 does not surpass the absolute SNL at the 1 photon per bit; it does reach its absolute quantum advantage for the input energies in the approximate range from 1.5 to 5 photons per bit and beats the absolute SNL by ≈ 1 dB. Our receiver's advantage over the previous record is due to photon detection time-resolving capability. We are not aware of any other quantum receivers that surpass the absolute SNL for any $M>4$ alphabets in the telecom band.

B. Energy-bandwidth optimization

To evaluate the joint energy-bandwidth properties of our communication schemes, we calculate the spectral efficiency (SE) and experimentally obtain the energy consumption (EC) for a fixed SER. Conventionally, spectral efficiency is defined as information rate, $\log_2 M$ (bits s^{-1}) over unit bandwidth, B (Hz), and $SE=\log_2 M/B$.

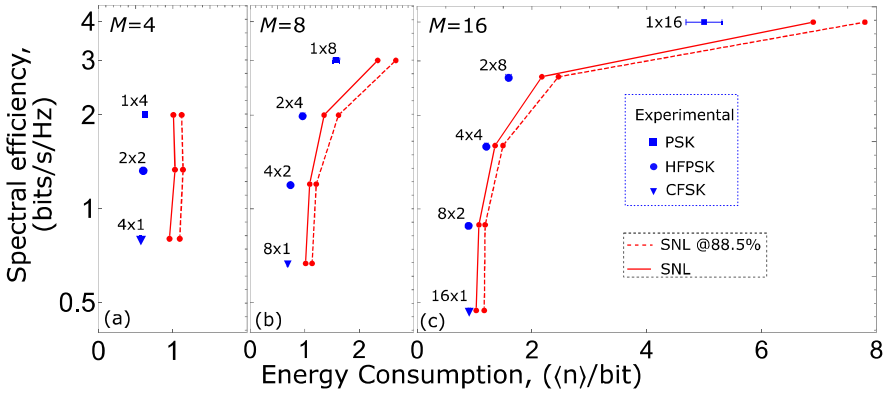

Fig. 4. Spectral efficiency (SE) vs experimentally measured energy consumption (EC) at SER = 15% for alphabet length (a) $M=4$, (b) $M=8$, and (c) $M=16$. Solid triangle, circle, and square markers represent the CFSK, HFPSK, and PSK modulation schemes, respectively. The red solid dots connected with solid lines and dashed lines represent the absolute SNL and the adjusted SNL for our system efficiency, respectively. All connecting lines are guides for the eye.

The unit of measurement is bits s^{-1} Hz^{-1}. The SE for the protocols considered here can be written as

$$\mathrm{SE} = \frac{\log_2(M_\mathrm{f} \times M_\mathrm{ph})}{1 + \left[(M_\mathrm{f} - 1)\dfrac{\Delta\omega T}{2\pi}\right]}, \tag{1}$$

where $\Delta\omega T$ is the detuning parameter.[11]

The EC is defined as the average number of photons required to transmit a bit with the desired SER,

$$\mathrm{EC} = \frac{\langle n\rangle|_\mathrm{SER}}{\log_2(M)}, \tag{2}$$

where $\langle n\rangle$ is the average number of photons per symbol. The unit of measurement of EC is the average number of photons per bit. Using the energy per bit rather than energy per symbol offers a direct energy requirement comparison between alphabets with different M. As defined, EC characterizes the information capacity of a communication channel only and not the energy required to operate the entire communication system. While the former is a fundamental physical property of a communication channel, the latter depends on implementation and is outside the scope of the manuscript.

In Fig. 4, we plot SE versus EC to experimentally demonstrate the trade-offs in the resource use for different alphabet lengths $M = 4$, 8, and 16. We show the results at SER = 15%. It is evident from the figure that all the experimental data points unconditionally outperform the SNL by the EC. The result shows that with the increment of alphabet length, from $M=4$ to 16, the EC improves for CFSK and the SE improves for PSK. Therefore, CFSK has the lowest EC for the same error rate compared to other modulations and PSK has the best SE. For $M=4$, the penalty in EC for PSK is very small compared to other modulations. In contrast, for $M>4$, the penalty in EC for PSK modulation grows very rapidly even when a quantum telecom receiver is used. Interestingly, this rapid growth of EC penalty can be significantly reduced with a small expansion into the bandwidth by using the HFPSK encoding ($M_\mathrm{f} \times M_\mathrm{ph} = 2 \times 8$-HFPSK). Here, 70% reduction of energy consumption at the expense of a 30% reduction in spectral efficiency can be achieved in comparison to 16-PSK. If the goal is reducing the bandwidth, then one can use the HFPSK encoding ($M_\mathrm{f} \times M_\mathrm{ph}$

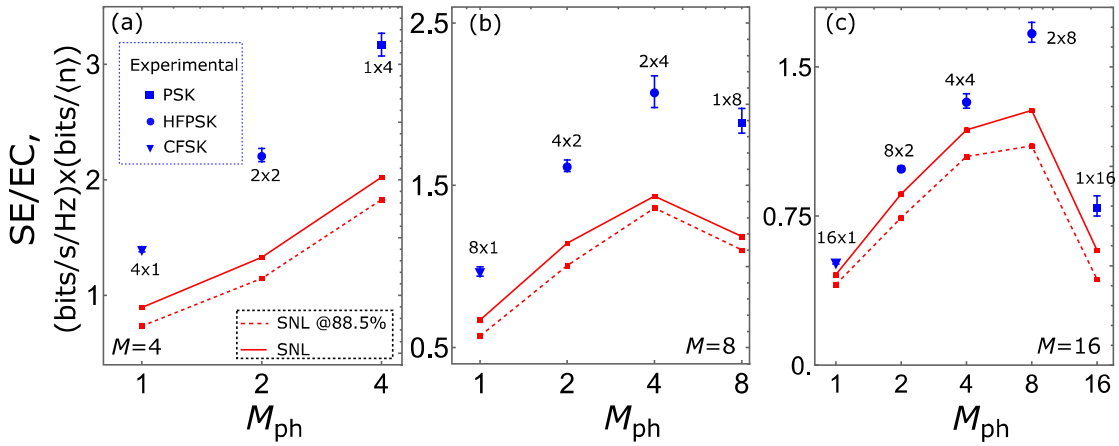

Fig. 5. Combined resource efficiency, SE/EC, at SER = 15% plotted against number of phase states, M_{ph}, for alphabet length (a) $M=4$, (b) $M=8$, and (c) $M=16$. Solid triangle, circle, and square markers represent the CFSK, HFPSK, and PSK modulation schemes, respectively. The red solid dots connected with solid lines and dashed lines represent the absolute SNL and the adjusted SNL for our system efficiency, respectively. All connecting lines are guides for the eye.

$= 8 \times 2$-HFPSK) and it can increase the spectral efficiency nearly by the factor of two with almost same EC as 16-CFSK.

C. Combined resource efficiency

There exists a trade-off between bandwidth and energy use. This trade-off can be quantified by a combined resource use cost function. Here, we assume that both bandwidth and energy are equally important resources and introduce the combined resource efficiency as SE/EC. In Fig. 5, we plot SE/EC against the number of phase states, ($M_{\mathrm{ph}} = M/M_{\mathrm{f}}$) for the same protocols as in Fig. 4. We also compared our experimental results with the theoretical SNLs. We show that the combined resource use of a quantum receiver is better than that of any classical receiver for all the communication protocols that we studied. We experimentally determine that the HFPSK has the highest combined resource efficiency for longer alphabets ($M = 8$ and 16) compared to other modulation schemes with the same M.

V. CONCLUSION

In conclusion, we demonstrate the first quantum receiver at the telecom wavelength that enables a range of modulation schemes with alphabet lengths $M \leq 16$. The experimental results show that all the encodings attain SERs below the SNL unconditionally, enabling the quantum advantage at telecom wavelengths. Also, the best quantum advantage of our receiver at the average input energy of 1 photon/bit is 3.4 dB more than the best quantum advantage of the previously demonstrated telecom receiver for the $M = 4$ PSK protocol.[27] We show that fundamental resources, such as energy and bandwidth, can be optimized as required by the application by choosing the appropriate encoding. In addition, we use the combined resource efficiency as a performance index for an arbitrary modulation scheme. We demonstrate that HFSPK modulation schemes have the highest combined resource efficiency. With our receiver design, different modulations and different alphabet lengths are enabled by changing the FPGA firmware with no modification to the optical setup. Thus, encodings can be changed dynamically depending on the optimization objective of the practical network. Our results show that our telecom versatile quantum receiver can be practically used for classical telecommunication to tame the physical resource needs beyond the capabilities of any classical receiver.

ACKNOWLEDGMENTS

This work was partially supported by the National Science Foundation through ECCS 1927674.

AUTHOR DECLARATIONS

Conflict of Interest

The authors have no conflicts to disclose.

Author Contributions

M. V. Jabir: Conceptualization (equal); Data curation (lead); Formal analysis (lead); Methodology (lead); Validation (lead); Writing – original draft (equal). **N. Fajar R. Annafianto:** Formal analysis (supporting); Software (lead). **Ivan Burenkov:** Conceptualization (equal); Data curation (supporting); Methodology (supporting); Software (supporting); Validation (supporting); Writing – original draft (equal). **Mario Dagenais:** Investigation (supporting); Resources (supporting). **Abdella Battou:** Funding acquisition (equal); Resources (supporting). **Sergey V. Polyakov:** Conceptualization (lead); Funding acquisition (equal); Investigation (supporting); Resources (equal); Supervision (lead); Writing – original draft (equal).

DATA AVAILABILITY

The data that support the findings of this study are available from the corresponding author upon reasonable request.

APPENDIX A: INTERFERENCE VISIBILITY

We measured the visibility by recording the beat note of two near-frequency inputs (signal and LO) in a transmitter–receiver arrangement. Figure 6 shows the histogram of photon detection times during the measurement period $T = 65.5$ μs accumulated over 150 s. The measured visibility is 99.4%.

APPENDIX B: THE TOTAL SYSTEM EFFICIENCY ESTIMATION

We define the input to the quantum receiver as the optical signal in the fiber before it enters FBS-3, see gray arrow in Fig. 2. Thus, system efficiency calibration consists of calibrating two major components and is given by their product: (1) the combined transmittance through the FBS-3 and the polarization controller (PC) and (2) the detection efficiency of the SNSPD detector.

The transmittance of FBS-3 and PC is measured using a fiber-coupled optical power meter and is 0.925(2).

We follow the substitution with calibrated attenuators method to find the detection efficiency of SNSPD.[34] First, the attenuators are calibrated. We use a classical InGaAs photodiode to determine the attenuation factor of the two attenuators. The measured attenuation factors are 9010(40) and 935(7). The uncertainty is estimated as a statistical uncertainty. Then, we send laser light into the fiber-

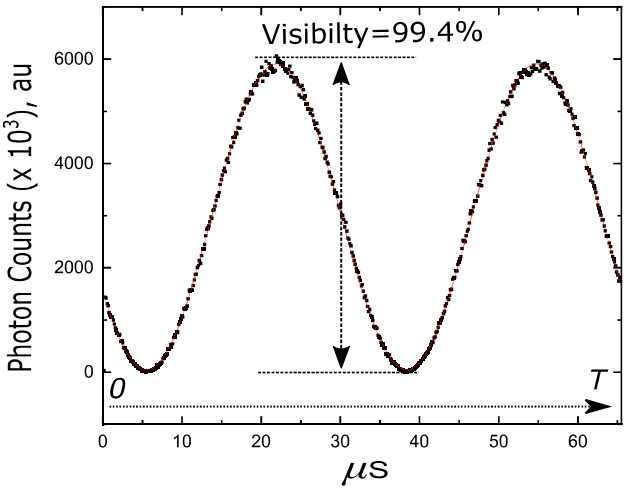

FIG. 6. The beat note of the two near frequency inputs to the transmitter–receiver arrangement is measured by a single-photon detector.

coupled calibrated InGaAs photodiode and measure its output using a trans-impedance amplifier. We note that the InGaAs photodiode detection efficiency of 0.805(1), the transmittance of the InGaAs photo-diode coupler is 0.953(3), and the gain of the trans-impedance amplifier is 10^7 V/A. Then, the optical input to the classical photodiode through PC is attenuated with the calibrated attenuators and the photodiode is substituted with the fiber-coupled SNSPD. Also, the polarization of the laser light is optimized to maximize the detection efficiency at the SNSPD detector using the PC. The output power measured using the InGaAs detector is converted to the average photon number at ≈1550 nm and compared with the measured average photon number from the SNSPD. The ratio between the measured photon number and the converted input average photon number gives the detection efficiency of the SNSPD. We repeated the same measurement for three different laser powers and obtained an average detection efficiency of 0.957(5). The maximal contribution to this uncertainty is the statistical uncertainty of calibrating the attenuators.

Therefore, the total system efficiency is 0.885(5), its uncertainty is mainly due to the statistical uncertainty of calibrating the attenuators. This measured total system efficiency is used throughout the manuscript.

REFERENCES

[1]C. W. Helstrom, J. Stat. Phys. **1**, 231 (1969).
[2]S. J. Dolinar, "An optimum receiver for the binary coherent state quantum channel," Report No. 111 (Research Laboratory of Electronics, MIT, 1973).
[3]D. Sych and G. Leuchs, Phys. Rev. Lett. **117**, 200501 (2016).
[4]M. P. da Silva, S. Guha, and Z. Dutton, "Achieving minimum-error discrimination of an arbitrary set of laser-light pulses," Phys. Rev. A **87**(5), 052320 (2013).
[5]R. S. Kennedy, "A near-optimum receiver for the binary coherent state quantum channel," Report No. 108 (Research Laboratory of Electronics, MIT, 1972).
[6]R. S. Bondurant, Opt. Lett. **18**, 1896 (1993).
[7]S. J. Dolinar, "A near-optimum receiver structure for the detection of M-ary optical ppm signals," The Telecommunications and Data Acquisition Progress Report No. 42-72, 1982.
[8]J. Chen, J. L. Habif, Z. Dutton, R. Lazarus, and S. Guha, Nat. Photonics **6**, 374 (2012).
[9]F. E. Becerra, J. Fan, G. Baumgartner, S. V. Polyakov, J. Goldhar, J. T. Kosloski, and A. Migdall, Phys. Rev. A **84**, 062324 (2011).
[10]C. R. Müller and C. Marquardt, New J. Phys. **17**, 032003 (2015).
[11]I. A. Burenkov, O. V. Tikhonova, and S. V. Polyakov, Optica **5**, 227 (2018).
[12]K. Tsujino, D. Fukuda, G. Fujii, S. Inoue, M. Fujiwara, M. Takeoka, and M. Sasaki, Opt. Express **18**, 8107 (2010).
[13]K. Tsujino, D. Fukuda, G. Fujii, S. Inoue, M. Fujiwara, M. Takeoka, and M. Sasaki, Phys. Rev. Lett. **106**, 250503 (2011).
[14]K. Kato, M. Osaki, M. Sasaki, and O. Hirota, IEEE Trans. Commun. **47**, 248 (1999).
[15]Y. Zuo, K. Li, and B. Zhu, MATEC Web Conf. **61**, 06008 (2016).
[16]F. Becerra, J. Fan, G. Baumgartner, J. Goldhar, J. Kosloski, and A. Migdall, Nat. Photonics **7**, 147 (2013).
[17]F. Becerra, J. Fan, and A. Migdall, Nat. Photonics **9**, 48 (2015).
[18]M. T. DiMario and F. E. Becerra, Phys. Rev. Lett. **121**, 023603 (2018).
[19]M. DiMario, L. Kunz, K. Banaszek, and F. Becerra, npj Quantum Inf. **5**, 65 (2019).
[20]S. Izumi, J. S. Neergaard-Nielsen, and U. L. Andersen, Phys. Rev. Lett. **124**, 070502 (2020).
[21]A. R. Ferdinand, M. T. DiMario, and F. E. Becerra, npj Quantum Inf. **3**, 43 (2017).
[22]I. A. Burenkov, M. V. Jabir, N. F. R. Annafianto, A. Battou, and S. V. Polyakov, "Experimental demonstration of time resolving quantum receiver for bandwidth and power efficient communications," in *Conference on Lasers and Electro-Optics* (Optical Society of America, 2020), p. FF1D.1.
[23]I. Burenkov, M. Jabir, A. Battou, and S. Polyakov, PRX Quantum **1**, 010308 (2020).
[24]M. V. Jabir, I. A. Burenkov, N. F. R. Annafianto, A. Battou, and S. V. Polyakov, OSA Continuum **3**, 3324 (2020).
[25]I. A. Burenkov, N. F. R. Annafianto, M. V. Jabir, M. Wayne, A. Battou, and S. V. Polyakov, Phys. Rev. Lett. **128**, 040404 (2022).
[26]M. L. Shcherbatenko, M. S. Elezov, G. N. Goltsman, and D. V. Sych, Phys. Rev. A **101**, 032306 (2020).
[27]S. Izumi, J. S. Neergaard-Nielsen, S. Miki, H. Terai, and U. L. Andersen, Phys. Rev. Appl. **13**, 054015 (2020).
[28]L. Mandel and E. Wolf, *Optical Coherence and Quantum Optics* (Cambridge University Press, 1995).
[29]I. A. Burenkov, M. V. Jabir, and S. V. Polyakov, AVS Quantum Sci. **3**, 025301 (2021).
[30]M. V. Jabir, N. F. R. Annafianto, I. A. Burenkov, A. Battou, and S. V. Polyakov, npj Quantum Inf. **8**, 63 (2022).
[31]A. D. Ellis, N. M. Suibhne, D. Saad, and D. N. Payne, Philos. Trans. R. Soc. A **374**, 20150191 (2016).
[32]E. A. Donley, T. P. Heavner, F. Levi, M. O. Tataw, and S. R. Jefferts, Rev. Sci. Instrum. **76**, 063112 (2005).
[33]T. Zhu, Y. Hu, P. Gatkine, S. Veilleux, J. Bland-Hawthorn, and M. Dagenais, IEEE Photonics J. **8**, 16362489 (2016).
[34]I. Mueller, R. D. Horansky, J. H. Lehman, S. Nam, I. Vayshenker, L. Werner, G. Wuebbeler, and M. White, Opt. Express **25**, 21483 (2017).
[35]S. Guha, J. L. Habif, and M. Takeoka, J. Modern Opt. **58**, 257 (2011).